DCS

Center for Nuclear Waste Regulatory Analyses

6220 CULEBRA ROAD • P.O. DRAWER 28510 • SAN ANTONIO, TEXAS, U.S.A. 78228-0510
(210) 522-5160 • FAX (210) 522-5155

June 27, 1995
Contract No. NRC-02-93-005
Account No. 20-5702-723

U.S. Nuclear Regulatory Commission
ATTN: Mr. T.J. McCartin
Performance Assessment & Hydrology Branch
Mail Stop T7D-13
Washington, DC 20555

Subject: Re-Transmittal of Intermediate Milestone 20-5702-723-530: Paper on Near-Field Coupled Liquid, Vapor, and Heat Transport

Dear Mr. McCartin:

The subject paper, entitled "Quasi-Steady State Model for Coupled Liquid, Vapor, and Heat Transport: Application to the Proposed Yucca Mountain High-Level Waste Repository," was previously submitted to fulfill an intermediate milestone. In preparing copies of the paper for transmittal to the NRC, one figure was inadvertently omitted. Attached please find a copy of the paper with the complete set of figures.

If you have any questions, please contact me at (210) 522-3805 or Dr. Peter Lichtner at (210) 522-6084.

Very truly yours,

Robert G. Baca, Manager
Performance Assessment

Delete all dist except: File PDR Full Rept

RGB/mag
f:Quasi.ltr
Attachment
cc: J. Linehan
S. Fortuna
B. Stiltenpole
B. Meehan
J. Greeves
M. Federline
J. Austin
K. McConnell
N. Eisenberg
D. Codell
R. Wescott
P. Justus
D. Dancer
S. Bahadur
J. Randall
R. Cady
W. Patrick
CNWRA Directors
CNWRA Element Managers
R. Manteufel
P. Lichtner
S. Rowe

NH15.11
426.1
WM-11

Washington Office • Crystal Gateway One, Suite 1102 • 1235 Jefferson Davis Hwy. • Arlington, Virginia, 22202-3293

QUASI-STEADY STATE MODEL FOR COUPLED LIQUID, VAPOR, AND HEAT TRANSPORT:

Application to the Proposed Yucca Mountain High-Level Waste Repository

by

John C. Walton

Department of Civil Engineering

University of Texas at El Paso

El Paso, TX 79968-0510

and

Peter C. Lichtner

Center for Nuclear Waste Regulatory Analyses

Southwest Research Institute

San Antonio, TX 78238-5166

May 18, 1995

Contents

ABSTRACT

A mathematical model based on the quasi-steady state approximation is developed to analyze liquid and water vapor transport near a heat source in the unsaturated zone. The model provides a simultaneous description of conductive heat transfer, unsaturated liquid flow, and diffusion and diffusion-caused-advection of water vapor and air. Temperature, liquid saturation, water fluxes, relative humidity, and evaporation rates are calculated as functions of radial distance for several specified times. The model is implemented using *Mathematica* software and applied to the very-near-field environment at the proposed high-level nuclear waste repository at Yucca Mountain, Nevada. It is shown that a limiting case solution exists where the vapor pressure of water is constant. For this case, the thermohydrology of the system can be determined without precise specification of hydraulic properties of the media. Granular materials placed as backfill around the container are shown to lead to the limiting case solution with enhanced dry out (low relative humidity) near the waste container, even at temperatures well below boiling. The model provides a method for assessment of the thermohydrology and design analysis of a single waste package.

1. INTRODUCTION

Simultaneous transport of liquid water and water vapor in response to temperature gradients occurs in a variety of situations in the unsaturated zone including near-surface solar heating of soils, disposal facilities for nuclear waste, and in the soil surrounding solar ponds. One example is the proposed repository for high-level nuclear waste (HLW) in the U.S. where heat generating waste would be placed in partially saturated tuffaceous rock at Yucca Mountain (YM), Nevada. The hydrothermal effects of heat-generating waste at the proposed repository have been investigated using numerical models describing transient two-phase flow and transport of water and air in liquid and gas phases (Pruess et al., 1990; Buscheck and Nitao, 1992). The overall effect is to create a dry-out zone around the repository and a zone of reduced vapor pressure near the waste package (Pruess and Tsang, 1994). The zone of dry-out and reduced vapor pressure leads to transport of water vapor away from the waste package by diffusion and bulk flow with condensation at distance and flow of liquid water toward the waste package resulting from capillary suction. The repository-scale calculations predict a quasi-steady state temperature profile after sufficient time has elapsed depending on the thermal loading, dominated by conduction away from the radioactive heat source (Pruess and Tsang, 1994; Lichtner and Walton, 1994).

Most previous model calculations of the proposed YM high-level waste (HLW) repository have been based at the repository-scale in which the individual waste packages are smeared out to form a uniform distribution of waste. These calculations are thus not able to describe moisture and heat redistribution in the vicinity of a single waste package. Nor are these calculations sensitive to the details of the waste package

geometry, and thus it is not possible to distinguish between different waste package designs which give the same repository-scale thermal loading. Nitao (1988) has analyzed a single waste package based on an infinite periodic array of waste packages. However, to take into account actual waste package emplacement presents enormous computational difficulties. The purpose of this contribution is to examine thermohydrologic conditions in the vicinity of a single waste package, referred to as the very-near-field to distinguish it from the near-field, the region impacted by the thermal perturbation at the repository scale. The waste package is assumed to be embedded in the thermalhydrologic field generated by the repository-scale configuration of smeared out waste. The quasi-steady state approximation is used to describe coupled liquid, vapor and heat transport for the proposed HLW repository at YM.

Coupled moisture and heat transport have been evaluated in models by Philip and deVries (1957) and deVries (1958). The vapor flux equation was further refined by Jury and Letey (1979), leading to the concept of enhanced vapor diffusion. This work follows the same basic governing equations for calculating vapor diffusion taking into account vapor pressure lowering and liquid advection governed by Darcy's law. The resulting equations are applied to steady-state conditions. The solution facilitates rapid assessment of the thermohydrologic conditions near a waste package and how these conditions relate to design of the waste package environment.

Thermohydrologic conditions in the very-near-field environment of the waste package are of critical importance in controlling container corrosion, leaching, and transport of radionuclides in the liquid or gas phase. Important considerations for the proposed repository are how the amount of waste loading per container and the presence or absence of backfill materials affect overall performance. For example, is it preferable to have a larger number of small waste containers or fewer larger containers? Is it preferable to place backfill material around the containers? Of special interest is the limiting case solution in which the vapor pressure of water in the system becomes constant and relative humidity and matric potential are a function of temperature only.

2. GOVERNING EQUATIONS AND SIMPLIFYING ASSUMPTIONS

The quasi-steady state approximation is based on the assumption that the region near a high-level waste package closely approximates a steady state, even as thermohydrologic conditions change over time at both the repository (hundreds of meters) and waste package scale (meters). The existence of a quasi-steady state requires that the rate of approach to steady state is rapid, relative to long-term changes related to waste decay and reduced thermal output. At steady state, liquid and vapor fluxes of water must be equal and opposite. Liquid water moves toward the waste package resulting from matric potential gradients, and vapor moves away from the waste container driven by vapor pressure gradients. When matric potential gradients are high, as is the case near the waste package, gravity effects can be ignored (Udell, 1983). Sufficiently close to the

waste package (i.e. at distances much less than the spacing between waste packages), transport is expected to be predominantly in the radial direction, allowing a one-dimensional simulation. The above simplifying assumptions lead to a single, explicit expression for the change of matric potential with distance. With appropriate boundary conditions derived from a repository-scale model, this equation can be integrated to determine the thermohydrologic properties of the system with distance and time.

2.1. Liquid and Gas Fluxes

Liquid flow is given by Darcy's law. We make the simplifying assumption that gravity can be neglected compared to matric potential gradients. In a cylindrically symmetric coordinate system the Darcy velocity for liquid water in a partially saturated porous medium is given by

$$v_l = -K\frac{d\psi}{dr} = -\frac{kk_r^l\rho_l g}{\mu_l}\frac{d\psi}{dr}, \tag{1}$$

where

v_l – specific discharge (Darcy velocity) (m/s),

ψ – matric potential of liquid water (m),

K – hydraulic conductivity (m/s),

k – absolute permeability (m^2),

k_r^l – liquid relative permeability, a function of ψ and material type (dimensionless),

ρ_l – density of liquid water, a function of temperature (kg/m^3),

μ_l – viscosity of liquid water, a function of temperature ($Pa \cdot s$),

g – acceleration of gravity (9.8 m/s^2),

r – radial coordinate (m).

Relative permeability k_r^l is a function of matric potential ψ using the van Genuchten relations (van Genuchten, 1980). Hydraulic conductivity K is obtained from permeability k, relative permeability k_r^l, density ρ_l, and viscosity μ_l of water at the local temperature according to Eq. (1).

The molar gas phase flux is equal to the sum of Fick and Darcy contributions. The total fluxes for air (a) and water (w), N_w^g and N_a^g, can be expressed as

$$N_w^g = J_w^g + F_w^g, \tag{2}$$

and

$$N_a^g = J_a^g + F_a^g, \tag{3}$$

respectively, where J_i^g represents the diffusive component of the flux and F_i^g the remaining contribution from the bulk flow of gas due to the presence of a pressure gradient for the subscripted species. The diffusive flux is based on Fick's law modified to account for enhanced vapor diffusion in a partially saturated environment given by the expressions:

$$J_w^g = -\frac{DP}{RT}\nabla X_w^g, \tag{4}$$

and

$$J_a^g = -\frac{DP}{RT}\nabla X_a^g, \tag{5}$$

where D denotes the effective binary diffusion coefficient for water vapor and air, X_i^g refers to the mole fraction of the subscripted species, P refers to the total gas pressure, R denotes the gas constant, and T the temperature.

Diffusion of water vapor through a porous media is complicated by the condensable nature of water. For a condensable gas such as water vapor, the diffusion rate in soils has been shown to be accelerated (Jury and Letey, 1979). As a consequence, the effective diffusion coefficient for water vapor in a porous rock is represented as:

$$D = \omega(\tau\phi)D_{aw}, \tag{6}$$

where ω represents an acceleration factor for water vapor diffusion relative to diffusion of other gases, τ denotes the tortuosity/constrictivity factor, ϕ denotes the porosity, and the binary diffusion coefficient for air/water vapor D_{aw} is taken as

$$D_{aw} = 2.1 \times 10^{-5}\left(\frac{P_0}{P}\right)\left(\frac{T}{298.15}\right)^{1.8}, \tag{7}$$

where $P_0 = 1.013 \times 10^5$ (Pa). Measurements in soils suggest that the effective diffusion coefficient is independent of the gas saturation S_g (Jury and Letey, 1979).

The nonsegregative component to the gas flux is described by Darcy's law with the form

$$F_w^g = -\frac{kk_r^g}{\mu_g}\frac{X_w^g P}{RT}\nabla P, \tag{8}$$

and

$$F_a^g = -\frac{kk_r^g}{\mu_g}\frac{X_a^g P}{RT}\nabla P, \tag{9}$$

for water vapor and air, respectively, where k_r^g denotes the relative permeability of the gas phase, μ_g refers to the viscosity, and the ideal gas law has been invoked. An expression for the total water vapor flux can be derived in which the nonsegregative component to the flux does not occur explicitly. It follows that

$$F_g = F_w^g + F_a^g = -\frac{kk_r^g}{\mu_g}\frac{P}{RT}\nabla P. \tag{10}$$

Thus, alternatively one can write

$$F_w^g = X_w^g F_g, \tag{11}$$

and

$$F_a^g = X_a^g F_g. \tag{12}$$

The total gas flux is equal to the sum of the nonsegregative components according to the equation

$$N_g = N_w^g + N_a^g = F_w^g + F_a^g = F_g, \tag{13}$$

as follows from the defining relation for the diffusive flux, which must, by definition, satisfy the condition

$$J_w^g + J_a^g = 0. \tag{14}$$

This relation follows from the definition of mole fraction

$$X_w^g + X_a^g = 1. \tag{15}$$

Using of Eq. (13), the total water vapor flux can be expressed alternatively as

$$N_w^g = J_w^g + X_w^g F_g = J_w^g + X_w^g N_g = J_w^g + X_w^g (N_w^g + N_a^g). \tag{16}$$

Under the assumption that the system is in a steady state and assuming that the component of air dissolved in the liquid phase is negligible compared to its concentration in the gas phase, it follows that air is stagnant ($N_a^g = 0$). As a consequence Eq. (16) yields

$$N_w^g = \frac{J_w^g}{1 - X_w^g}. \tag{17}$$

This form of the flux implicitly includes the effects of a pressure gradient and thus accounts for both advective and diffusive transport. The flux grows without bound as $X_w^g \to 1$. This expression for the flux of water vapor is identical to that obtained by Bird et al. (1960), referred to as diffusion-caused-advection. The ratio of the Darcy to the diffusive flux for water vapor is equal to

$$\frac{F_w^g}{J_w^g} = \frac{X_w^g}{1 - X_w^g}, \tag{18}$$

and thus in the limit $X_w^g \to 1$, the water vapor flux is dominated by bulk flow.

2.2. Water Vapor and Air Transport in the Absence of a Liquid Phase

Before proceeding to the more complicated case of coupled liquid and vapor transport, it is instructive to examine the solution to the steady-state transport equations for an isothermal gas phase consisting of water

vapor and air in the absence of a liquid phase. This problem is referred to as the Stefan problem (Bird et al., 1960), and is discussed in many textbooks on heat and mass transfer (e.g. Incropera and DeWitt, 1990). However, all of these derivations make the simplifying assumption that total pressure is constant, which is relaxed in the presentation which follows in which Darcy's law is used to describe bulk gas flow in a porous medium.

For evaporation from the surface of an infinitely long container in the form of a cylinder with radius r_0, and assuming radial symmetry (no gravity), the steady-state governing equations are

$$N_w^g = -\frac{DP}{RT}\frac{dX_w^g}{dr} - \frac{k}{\mu_g}\frac{X_w^g P}{RT}\frac{dP}{dr} = \frac{\mathcal{E}}{2\pi r}, \tag{19}$$

for water vapor, and

$$N_a^g = -\frac{DP}{RT}\frac{dX_a^g}{dr} - \frac{k}{\mu_g}\frac{X_a^g P}{RT}\frac{dP}{dr} = 0, \tag{20}$$

for air, which is assumed to be stagnant. In these equations, $\mathcal{E}$ represents the (constant) evaporation rate at the surface $r = r_0$ per unit container length, with units of moles/m/s. Adding these two equations gives the total flux

$$N_g = -\frac{k}{\mu_g}\frac{P}{RT}\frac{dP}{dr} = \frac{\mathcal{E}}{2\pi r}. \tag{21}$$

This equation can be immediately integrated to give

$$P(r) = \sqrt{P_L^2 + \frac{\mu_g RT\mathcal{E}}{\pi k}\ln\left[\frac{r_L}{r}\right]}, \tag{22}$$

where P_L, equal to atmospheric pressure, represents the pressure at the outer radius r_L.

The water vapor mole fraction satisfies the differential equation

$$N_w^g = -\frac{DP}{RT}\frac{1}{1 - X_w^g}\frac{dX_w^g}{dr} = \frac{\mathcal{E}}{2\pi r}. \tag{23}$$

Noting that DP=constant according to Eq. (7), this equation has the solution

$$\ln\left[\frac{1 - X_w^g(r)}{1 - X_w^g(r_0)}\right] = \frac{RT\mathcal{E}}{2\pi DP}\ln\frac{r_0}{r}. \tag{24}$$

Evaluating this equation at $r = r_L$, the evaporation rate $\mathcal{E}$ is obtained as

$$\mathcal{E} = \frac{2\pi DP}{RT}\frac{\ln\left[\frac{1 - X_w^g(r_L)}{1 - X_w^g(r_0)}\right]}{\ln\left[\frac{r_L}{r_0}\right]}. \tag{25}$$

Evaporation takes place if $\mathcal{E} > 0$, and it follows that $X_w^g(r_0) > X_w^g(r_L)$. Otherwise condensation occurs. According to these results for $\mathcal{E} > 0$, the pressure gradient drives bulk flow of water vapor and air radially

outward. For air to remain stagnant it must diffuse inward counterbalancing the outward bulk flow. Water vapor diffuses outward leaving the system and providing a net evaporation rate.

For a highly permeable medium $k \to \infty$, and $P(r) \to P_L = \text{constant}$. In this limit bulk flow becomes independent of permeability. The mole fraction X_w^g is independent of permeability according to Eq. (24), assuming it is fixed at the evaporation surface. Actually, for the case of evaporation, the partial pressure of water vapor is fixed at the surface of the container by the imposed temperature of the system. In this case, a transcendental equation is obtained for the evaporation rate $\mathcal{E}$ by combining Eqs.(25) and (22) and noting that $X_w^g = p/P$ with p the partial pressure of water vapor assuming ideal gas behavior. Increasing the permeability with a fixed partial pressure of water vapor at the container surface thus results in an increase in the water vapor mole fraction at the surface.

2.3. Governing Equations for Simultaneous Liquid and Gas Transport

In this section the steady-state flux equations for simultaneous liquid and vapor transport are derived. At steady state the transport equations for liquid and gas are given by

$$\nabla \cdot N_w^l = -E, \tag{26}$$

for liquid water, and for the gas phase

$$\nabla \cdot N_w^g = E, \tag{27}$$

for water vapor, and

$$\nabla \cdot N_a^g = 0, \tag{28}$$

for air, where E denotes the volume averaged evaporation/condensation rate taken as positive for evaporation and negative for condensation, in units of moles/m^3/s. The dissolved component of air in the liquid phase is neglected. Adding the first two equations eliminates the evaporation rate to give

$$\nabla \cdot \left(N_w^l + N_w^g \right) = 0. \tag{29}$$

At steady state with no sources or sinks of moisture and zero flux boundary condition at the one end of the computation domain, liquid and vapor fluxes of water must be equal and opposite at each point. Converting to units of kg/m^2/s and equating liquid and vapor flow per unit length of the waste container at any radial distance yields:

$$\rho_l v_l = -M N_w^g, \tag{30}$$

where M denotes the molecular weight of water (18 kg/kmole). Using the ideal gas law, and assuming constant total gas pressure, the expression for the water vapor flux reduces to:

$$N_w^g = -\frac{DP}{(1-X_w^g)\,RT}\nabla X_w^g \doteq -\frac{D}{(1-p/P)\,RT}\frac{dp}{dr}. \tag{31}$$

where the latter expression refers to a cylindrical coordinate system with r the radial distance measured from the center of a waste container, and p refers to the water vapor partial pressure. In terms of the matric potential and partial water vapor pressure, the condition for a steady state, Eq. (30), becomes

$$\frac{d\psi}{dr} = -\frac{MD}{RTK\rho_l\,(1-p/P)}\frac{dp}{dr} = -\beta\frac{dp}{dr}, \tag{32}$$

where the quantity β is defined by

$$\beta = \frac{MD}{RTK\rho_l\,(1-p/P)}. \tag{33}$$

In this equation the vapor flux is expressed in terms of the gradient in water vapor pressure as the driving force for diffusion, whereas the liquid flux describes liquid flow in terms of the matric potential gradient. Both advection and diffusion of water vapor are included in Eq. (32) with air assumed to be stagnant. It should be noted that, unlike the transient transport equations in which the saturation state of the porous medium occurs in the accumulation term, it does not explicitly enter the quasi-steady state equation. However, once the matric potential has been computed, the saturation can be obtained from the corresponding van Genuchten relation, for example.

The evaporation rate can be computed from the following equivalent expressions

$$E = -\frac{1}{r}\frac{d}{dr}\left(rN_w^l\right) = \frac{1}{r}\frac{d}{dr}\left(rN_w^g\right), \tag{34}$$

in cylindrical coordinates. At interfaces between two dissimilar materials the evaporation rate has a Dirac δ–function singularity. The temperature field T, matric potential ψ, and water vapor pressure p, must be continuous across the interface, but because of differing material properties in the two adjoining media their gradients have a jump discontinuity. Consequently, the flux has a jump discontinuity and can be represented in terms of the Heaviside function $\theta(\eta)$ as:

$$N = [1-\theta(r-r_l)]\,N^{(-)} + \theta(r-r_l)N^{(+)}, \tag{35}$$

where $N^{(-)}$ and $N^{(+)}$ denote the flux to the left and right of the interface located at r_l with

$$\theta(\eta) = \begin{cases} 1 & (\eta > 0) \\ 0 & (\eta < 0) \end{cases}. \tag{36}$$

Differentiating Eq. (35) gives

$$\frac{1}{r}\frac{d}{dr}(rN) = \delta(r-r_l)[N] + [1-\theta(r-r_l)]\frac{1}{r}\frac{d}{dr}\left(rN^{(-)}\right) + \theta(r-r_l)\frac{1}{r}\frac{d}{dr}\left(rN^{(+)}\right). \tag{37}$$

where $[N]$ denotes the jump in the flux across the interface

$$[N] = N^{(+)} - N^{(-)}. \tag{38}$$

Introducing the evaporation rate, Eq. (37) becomes

$$E = \delta(r - r_l)E_\delta + [1 - \theta(r - r_l)]E^{(-)} + \theta(r - r_l)E^{(+)}. \tag{39}$$

The first term on the right-hand side of Eq. (39), proportional to the Dirac δ–function, represents the contribution to the evaporation rate at the interface. The second two terms represent the contribution to the left and right of the interface, respectively. Note that the term E_δ has units of moles/m^2/s, whereas $E^{(\pm)}$ has the units moles/m^3/s.

2.4. Vapor Pressure Lowering

To integrate Eq. (32), it is necessary to eliminate one of the quantities ψ or p. If the water vapor pressure is confined to the saturation pressure curve, represented by the function $p^\circ(T)$, this would provide water vapor pressure as a function of temperature and hence radial distance. Another possibility explored in more detail in this section is the use of the Kelvin equation describing vapor pressure lowering resulting from capillary and adsorptive forces. The matric potential ψ and water vapor pressure p both express the activity of water in the system and are related through Kelvin's equation:

$$p = p^\circ(T) \exp\left(\frac{\psi M g}{RT}\right). \tag{40}$$

Use of this equation results in a differential equation for a single unknown p or ψ. As pointed out by Pruess et al. (1990), for strong suction one must be careful in interpreting this equation in terms of the usual explanation of the curvature of matrix pores, which would require impossibly small radii. Rather, in such cases the Kelvin equation must be interpreted in terms of surface adsorption of liquid water (Philip, 1978). The vapor pressure of pure water p computed using the Kelvin equation is shown in Figure 1 as a function of temperature and ψ. The contour lines range from 0.1 to 1 atm. For extremely large values of ψ the curves must be used with caution. As the vapor pressure of water approaches the local atmospheric pressure, the bulk flow enhancement factor, $1/(1 - p/P)$, approaches infinity as shown in Figure 2, leading to rapid water vapor transport and increased drying of the system.

Differentiating the Kelvin equation yields the following expression for the derivative of vapor pressure with radial distance

$$\frac{d \ln p}{dr} = \frac{Mg}{RT}\frac{d\psi}{dr} + \left[\frac{d \ln p^\circ}{dT} - \frac{Mg\psi}{RT^2}\right]\frac{dT}{dr}. \tag{41}$$

Substituting this expression into the mass conservation equation, Eq. (32), and solving the resulting expression for $d\psi/dr$ yields

$$\frac{d\psi}{dr} = -\frac{\alpha}{1+\alpha}\frac{RT}{Mg}\left[\frac{d\ln p^\circ}{dT} - \frac{Mg\psi}{RT^2}\right]\frac{dT}{dr}. \tag{42}$$

where the dimensionless quantity α is defined by

$$\alpha = \frac{pMg}{RT}\beta, \tag{43}$$

with β defined in Eq. (33). Equation (42) represents a nonlinear, ordinary differential equation for the matric potential for a given superimposed temperature profile.

The quantity α can be viewed as the ratio of the coefficients controlling water vapor transport to those controlling liquid water transport. Liquid and vapor fluxes are proportional to the gradient in ψ (Eq. (1)) or p (Eq. (31)), respectively. Because the fluxes of water vapor and liquid water are constrained to be equal and opposite, as α approaches the extreme values 0 or ∞, either constant p ($\alpha \gg 1$) or constant ψ ($\alpha \ll 1$) results. For $\alpha \ll 1$, it follows that

$$\frac{d\psi}{dr} \simeq 0, \tag{44}$$

and diffusion of water vapor becomes the rate controlling step. For $\alpha \gg 1$, the mass conservation equation reduces to

$$\frac{d\psi}{dr} = -\frac{RT}{Mg}\left[\frac{d\ln p^\circ}{dT} - \frac{Mg\psi}{RT^2}\right]\frac{dT}{dr}. \tag{45}$$

Comparing this result with Eq. (41) derived from the Kelvin equation, leads to the requirement

$$\frac{dp}{dr} \simeq 0, \tag{46}$$

that the vapor pressure of water be approximately constant. In this case flow of liquid water becomes the rate controlling step. It should be noted that this result is not inconsistent with Eq. (32) because in the limit $\alpha \to \infty$, it follows that $\beta \to \infty$ also, and thus Eq. (32) reduces to

$$\frac{d\psi}{dr} = -\infty \cdot 0, \tag{47}$$

an indeterminate form. Thus, for finite but large values of α the vapor pressure of water is effectively constant, but in a strict sense increases slightly towards the waste container in order to maintain a nonzero vapor flux. For $\alpha \gg 1$, it follows directly from the Kelvin equation that the matric potential is given explicitly by the expression

$$\psi(r) = \frac{RT}{Mg}\ln[h(r)], \tag{48}$$

where $h(r)$ represents the relative humidity defined by

$$h(r) = \frac{p}{p^{\circ}[T(r)]}. \tag{49}$$

Thus when $\alpha \gg 1$, the vapor pressure of water in the system can be considered effectively constant, and matric potential and relative humidity are simple functions of temperature. In practice at large α, the gradient in vapor pressure becomes indeterminate and an identical solution for ψ is obtained with the simplified limiting case solution. When the limiting case is assumed in the numerical integration, the equal and opposite liquid and vapor fluxes can be obtained directly from Eq. (1) using the matric potential from Eq. (48).

2.5. Temperature Field

For the system under consideration, the boundary conditions imposed on the problem are, in general, a time-dependent heat generation rate resulting from radioactive decay at the inner boundary r_1 (e.g., waste container boundary), and a specified time-dependent temperature and matric potential, representing the repository-scale temperature and matric potential fields, at the outer boundary r_3. The heat generation rate and outer temperature and matric potential are assumed to change sufficiently slowly with time resulting in formation of a quasi-steady state. At steady state, the heat transfer rate is the same throughout the system giving:

$$\frac{Q(t)}{2\pi r} = -\kappa \frac{dT}{dr}, \tag{50}$$

where

$Q(t)$ – thermal energy per unit length of waste container resulting from radioactive decay (J/s/m),

κ – thermal conductivity for backfill and host rock, a function of material type and in general, matric potential or equivalently saturation (W/m/K).

Because of the small amounts of water anticipated to contact the container subsequent to the initial thermal transient and in the absence of heat pipe formation, the loss of sensible and latent heat by water heating and evaporation from the container surface at later time periods (>100 years) is insignificant in the overall energy balance. Additionally, at low water content, thermal conductivity is independent of moisture content. In this case, heat transfer is independent of moisture content and the temperature can be calculated directly by analytical solution (i.e, one-dimensional, radial, steady-state heat conduction in a layered medium). With the temperature known, Eq. (42) can be integrated directly as a single ordinary differential equation. If advective transfer of heat is important and/or if thermal conductivity is a strong function of moisture content, then solution of the ordinary differential equation for temperature (Eq. (50)) must be coupled with the solution of Eq. (42) (and additional heat transfer terms must be added to Eq. (50)).

For the simple case of heat conduction only, integration of Eq. (50) gives:

$$T(r;t) = \begin{cases} \dfrac{Q(t)}{2\pi\kappa_r}\ln\left(\dfrac{r_3}{r}\right) + T_3(t), & (r_2 \le r \le r_3), \\ \dfrac{Q(t)}{2\pi\kappa_b}\ln\left(\dfrac{r_2}{r}\right) + \dfrac{Q(t)}{2\pi\kappa_r}\ln\left(\dfrac{r_3}{r_2}\right) + T_3(t), & (r_1 \le r \le r_2), \end{cases} \tag{51}$$

where

r_1, r_2, r_3 – radial distance of container surface, backfill/host rock interface, and outer boundary measured from container centerline (m),

$T_3(t)$ – outer boundary temperature at $r = r_3$ (K),

κ_b, κ_r – thermal conductivity of backfill and host rock, respectively.

The simplified conduction-only solution is used in all the simulations contained in this paper. The system is fully specified by integration of Eq. (42) with the temperature given by Eq. (51). Integration proceeds from the outer boundary, where a specified time-dependent matric potential and temperature are assumed, to the inner boundary at the waste container surface providing the matric potential as a function of radial distance. It should be noted that many of the parameters included in Eq. (42) are themselves a function of temperature, matric potential, and the properties of the porous media as indicated in the definitions of each parameter. The constitutive properties must all be specified prior to integration of the equation.

3. SIMULATIONS

In this section, the governing steady-state transport equation is applied to the very-near-field region of a waste package with time-dependent boundary conditions determined from a repository-scale model. In the vicinity of the waste package, the approach to a steady-state flux of liquid and vapor is presumed to be rapid relative to the time scales for radionuclide decay (100s to 1,000s of years), except for very early times when the decay heat changes more rapidly with time.

3.1. Input Data, Constitutive Properties, and Scenario Description

The simulation geometry for the very-near-field of a high-level radioactive waste package is depicted in Figure 3. Heat loads of 57 and 28.5 kW/acre are used in the calculations based on ten-year-old fuel for 70,000 metric tons of 60% pressure water reactor (PWR) fuel at 33,000 MWd/MTU burnup and 40% boiling water reactor (BWR) fuel at 27,500 MWd/MTU burnup (DOE, 1993). It is assumed that the region near the waste package can be represented in a radial geometry with a no-flux boundary condition at $r = 0$, the container

centerline. The waste package is assumed to consist of a long cylinder with radius r_1. The container is considered to be sufficiently long that end effects can be neglected, leading to a one dimensional problem with radial symmetry. Because the effects of gravity are ignored, vertical versus horizontal emplacement of the waste cannot be distinguished by the model.

Two materials are considered in the simulations, the host rock and backfill with the material properties listed in Table 1. The quantities n and a refer to the van Genuchten parameters in the expressions relating matric potential and relative permeability to liquid saturation. Residual saturation is assumed to be zero. The radii of the regions of different materials corresponding to the container, backfill, and host rock are given in Table 2. The backfill is assumed to have properties of GE sand (van Genuchten and Nielsen, 1985), and host rock properties are taken from Lichtner and Walton (1994) corresponding to the Topopah Spring stratigraphic unit at YM. The container material properties are assumed arbitrarily to be the same as the backfill. The container is optionally considered to be surrounded by a backfill material with radius r_2. The simulation extends through an outer layer of host rock to a maximum radius r_3.

An important characteristic of the host rock is the extent to which it holds water at high negative matric potential compared to the backfill material, which rapidly desaturates. The van Genuchten curve for relative permeability versus matric potential is shown in Figure 4 for the backfill material and host rock. Although the rock matrix has a much lower saturated permeability, the greater preponderance of smaller pores compared to pore sizes in likely backfill materials leads to a much lower attenuation of permeability with ψ. For this reason, at high negative matric potential, the rock matrix has a higher liquid permeability than the assumed backfill material.

The boundary conditions for T and ψ at r_3 used in the simulation are given in Table 3. The boundary conditions are obtained from a repository-scale model based on the equivalent continuum representation of fractured porous media using the code CTOUGH (Lichtner and Walton, 1994). Data for material properties of the tuff host rock are taken from Peters et al. (1984). An equivalent continuum permeability of 1.8×10^{-14} m^2 and porosity of 10 percent are used in the repository-scale calculations. Matrix permeability and porosity used are, respectively, 1.9×10^{-18} m^2 and 0.1; and fracture permeability and porosity of 10^{-11} m^2 and 0.0018, respectively. Initial conditions used in the repository-scale calculations are obtained by first computing a steady-state solution without the presence of a heat source and using this solution for the initial condition with the heat source present. The outer boundary temperature T_3 and matric potential ψ_3 depend only on overall repository thermal loading, not on the individual container geometry.

The experimental work of Ali et al. (1994) is used to estimate the tortuosity-porosity factor appearing in the effective diffusion coefficient. For YM tuff, this estimate results in a value of $\tau \sim 10^{-2}$ for the Topopah Spring unit assuming a porosity of approximately 10 percent. A value for the acceleration factor for YM tuff of $\omega = 10$ is obtained by extrapolating the data obtained by Jury and Letey (1979) for soils and assuming the

same acceleration factor to hold for YM tuff. Details are given in Lichtner and Walton (1994). The effective diffusion coefficient for water vapor in the tuffaceous host rock is represented as:

$$D = 10^{-2} D_{aw}. \tag{52}$$

For the backfill material the following expression is assumed to hold

$$D = 0.26 D_{aw}. \tag{53}$$

In order to stabilize liquid water at elevated temperatures, the vapor pressure of liquid water must be lowered. Vapor pressure lowering can occur from salinity (Walton, 1993; Walton, 1994) and/or from matric potential as demonstrated in Figure 1. The tuff rock matrix has a higher capability of holding water under tension compared to the backfill material (with assumed properties of sand), which has only a limited ability to hold moisture under a state of tension. This difference in material properties has a large and distinct effect on simulation results for the backfill and host rock.

3.2. Results and Discussion

Three different possibilities for repository waste package designs are simulated at two areal thermal loadings and at three different time periods resulting in a total of 18 different simulations. The simulations are defined and assigned labels in Table 4. Each curve in the results graphs is labeled with the appropriate simulation designation from Table 4. The small container design is based on the Site Characterization Plan (SCP) and is assumed to have 460 kg/(m of container length) of initial heavy metal (Department of Energy, 1993). The Multi-Purpose Canister (MPC) container is assumed to have 1,600 kg/m of initial heavy metal (Department of Energy, 1994).

Since final designs and adequate site characterization data have not been released by the YM project, the simulations are intended to represent only a parametric study comparing and contrasting several general options for the repository. The parameters investigated are (i) overall repository thermal loading, (ii) amount of waste per container, and (iii) influence of backfill material. In the simulations, all the liquid properties (viscosity, vapor pressure, density) and the diffusion coefficient are functions of temperature. Many of the parameters incorporated into Eqs.(42) and (50) or (51) are dependent upon temperature, matric potential, and the constitutive properties of the porous media through which the integration passes.

The governing equation is integrated using a Runge-Kutta algorithm with error controlled step sizes taken from *Numerical Recipes* (Press et al., 1986). Integration proceeds from the outer boundary, where the temperature T and matric potential ψ are assumed to be given as functions of time, toward the centerline of the waste container. The solution has the interesting property that material properties at smaller radial distances have no influence on the solution at greater radial distances.

3.2.1. Limiting Solution for $\alpha \gg 1$

Before presenting the results of the simulations for the solution to Eq. (42), it is useful to examine the limiting case $\alpha \gg 1$. The dimensionless quantity α for the case of tuff rock and backfill material is contoured in Figure 5 as a function of ψ and temperature. The limiting case is reached when $\alpha \geq 100$. Higher temperatures and highly negative matric potentials promote the limiting case solution. Major factors that control the value of α are the effective diffusion coefficient D as influenced by the bulk flow term $(1 - p/P)$, hydraulic conductivity K, and water vapor pressure p. The bulk flow enhancement factor $1/(1 - p/P)$ approaches infinity as the vapor pressure of water approaches atmospheric pressure, greatly enhancing water vapor transport (Figure 2). Density changes only slightly and the direct effect of temperature appears to be overshadowed by the indirect effect of temperature on water vapor pressure. The influence of ψ is also important since the hydraulic conductivity K is strongly dependent on ψ through the constitutive equation for relative permeability.

Several important observations can be obtained from this analysis. First, the backfill material is always within the limiting case (vapor pressure of water = effectively constant) for the range of anticipated matric potentials at YM, even at ambient temperatures, assuming the material properties of sand. Thus matric potential, relative humidity, and steady-state flux of moisture in the backfill can be estimated from a knowledge of ψ and T at the host rock/backfill interface. One should note that a more likely backfill/packing material than sand would be crushed tuff rock, most likely with a larger particle size than sand. Materials with a more coarse particle size than sand would tend to dry out more easily, leading more rapidly to the limiting case. Thus one can tentatively conclude that most crushed backfill materials would behave in a manner similar to sand and that precise knowledge of the hydraulic properties of the backfill/packing materials, as long as they are coarse, is not of great importance for estimating thermohydrologic conditions near the waste container. In contrast to the backfill material, the host rock holds moisture more tenaciously and only reaches the limiting case under highly negative matric potentials, for the assumed material properties. Thus good estimates of the unsaturated properties of the host rock are required for accurate predictions.

3.2.2. Temperature Gradients

Predicted very-near-field temperatures are presented in Figure 6 for each of the 18 simulations. The temperature calculations assume simple heat conduction in a one-dimensional radial system. Comparison of low and medium thermal loadings shows identical trends except that the temperatures are increased at greater thermal loading. Both the presence of backfill material with the thermal properties of dry sand and the MPC container with a greater amount of waste per container lead to higher waste package temperatures and higher thermal gradients near the waste. During early time periods, when temperature is greatest, convective cooling (not

included in this simulation) is likely to be important near the waste container. In a general design exercise, the thermal conductivity and gas permeability of the backfill could also be controlled to balance low relative humidity against peak temperatures, although this exercise is not carried out further here.

3.2.3. Moisture Content, Water Vapor Pressure, and Relative Humidity

The predicted relative humidity is presented in Figure 7. Relative humidity is perhaps the best measure of dry-out near the waste. Temperature gradients near the waste container can be as important as elevated temperature in controlling water dynamics. Lowering of the relative humidity results from steep temperature gradients near the waste and from the presence of the backfill material. The MPC with backfill always has significantly lower relative humidity than the other two designs. Even with lower temperature gradients caused by less fuel in the container compared to the MPC design, the smaller (SCP) container benefits from the presence of backfill material. The backfill material assists dry-out by forming an insulating layer around the waste promoting higher temperature gradients than without backfill, and because the granular material rapidly desiccates at highly negative matric potentials leading to the limiting case solution. However, one drawback to use of backfill may be the high temperatures that can be reached during the initial stages following waste emplacement. This aspect and the possible important role of localized convection in reducing peak temperatures cannot be investigated with the present approach.

After 10,000 years have elapsed and the repository has substantially cooled and heat output is low, the remaining thermal gradients near the waste are sufficient, when backfill material is used, to cause a large relative humidity depression near the waste. The drop in relative humidity maintains moisture tension gradients such that liquid water always moves towards the container. Even if the container has failed by this time, the advection of water towards the container effectively traps dissolved radionuclides in the vicinity of the waste. In order to support liquid releases, either water influx rates must be sufficient to overcome the moisture deficit in the backfill material, or water must be stabilized with soluble salts. The ability of soluble salts to stabilize water in the waste and on the waste container has been investigated by Walton (1993). Maximum vapor pressure lowering due to the presence of soluble salts is dependent upon the type of salt present and ranges from around 87% relative humidity for $NaCO_3$, 75% for NaCl, 60% for $NaNO_3$, and 22% for $CaCl_2$. Examination of Figure 7 suggests that, in the presence of granular backfill materials, the waste and waste container could remain dry for at least 1,000 years in the presence of calcium chloride.

In Figure 8 the predicted mole fractions of water for the 18 simulations are presented. Since total pressure is held constant, the mole fraction is proportional to water vapor pressure. The vapor pressure of water tends to be greater at higher repository thermal loading (higher average temperature). In the limiting case where $\alpha \gg 1$, the vapor pressure of water is constant corresponding to the horizontal portions of the curves. Although the limiting case is not always reached in the host rock, it is always reached in the backfill materials.

After the limiting case is reached, the hydraulic properties of the material are no longer needed with high precision to estimate relative humidity. Since the limiting case $\alpha \gg 1$ is generally reached in the backfill, the precise hydraulic properties of the backfill material are not important for predicting hydraulic conditions near the waste, at least for the first 10,000 years in the absence of salinity buildup.

3.2.4. Water Flux and Evaporation Rates

Water transport and evaporation are important because they are indicative of the rate of salinity buildup, leaching of the host rock, and precipitation of secondary minerals. Salinity buildup and precipitation of secondary minerals (e.g., silica, calcite) occur most strongly in evaporation regions. Leaching of the host rock occurs in regions of net condensation.

Liquid and vapor fluxes of water (left-hand side) and evaporation rates (right-hand side) are presented in Figures 9 and 10 for thermal loadings of 28.5 and 57 kW/acre, respectively. The evaporation rate shown in the figures is $2\pi r M$ times the evaporation rate as defined in Eq. (34). Condensation corresponds to a negative evaporation rate. Water flux is given in units of kg of water per second per unit length of the waste container and is obtained by differentiation of the ψ versus r curve obtained from the solution of the differential equation along with Darcy's law (Eq. (1)). The solution of the differential equation is expressed as an interpolation function in *Mathematica* (Wolfram, 1991), facilitating further calculations. The evaporation rate, expressed as kg of water per meter of radial direction per meter of container length per second, is obtained by differentiation of the water flux (see Eq. (34)).

The water flux and evaporation rate are only presented for the tuff host rock and not the backfill. Although it is possible to calculate flux rates in the backfill material, the relative permeabilities calculated with the van Genuchten expressions in the backfill are below 10^{-40} and can effectively be equated to zero. One should also remember that, because of the no-flux boundary condition at the center of the container, changes in material properties at smaller radii do not influence the numerical solution at greater radial distances. For this reason only two solutions are visible in the graphs since, for the SCP container with and without backfill, the calculations coincide until the backfill is reached (and the solution is not presented in the backfill).

As shown in Figure 9 for the 28.5 kW/acre thermal loading case, the water flux increases going toward the container for all time periods shown. All the evaporation curves are negative, indicating that condensation occurs throughout the rock, resulting in rewetting of the repository very-near-field. Possibly evaporation has taken place at earlier times not considered here when the heat release was greater. The greatest rate of condensation shown in the figures is near the rock/backfill or rock/container interface. The source of water for condensation is the water evaporated at the host rock/backfill or host rock/container interface. Although evaporation rates in the host rock can be significant, the major location for evaporation is actually at the material interface between the host rock and the backfill when backfill is present, and host rock/container when

backfill is not present. Evaporation rates across the interface, however, cannot be graphed because evaporation occurs right at the interface and would thus appear as a δ–function singularity (see Eq. (39)), and is therefore not shown in the figures. Estimated interfacial evaporation rates are listed in Table 5. Note the units of mass water/unit container length/unit time resulting from the δ–function singularity and the multiplicative factor $2\pi r M$.

The results for the water flux and evaporation rate at 57 kW/acre thermal loading are shown in Figure 10. In this case, evaporation does occur with a maximum evaporation rate at 500 years at a distance of about 1 m for the SCP container without backfill, and near 3 m for the MPC. At 1,000 and 10,000 years, condensation occurs throughout the rock indicating rewetting. More generally, extending from the waste package center, there is typically a zone of evaporation followed by a zone of condensation. Over time the zone of condensation moves towards the edge of the host rock, where the evaporation rate is proportional to a Dirac δ–function. This trend would tend to "sweep" the accumulated soluble salts towards the waste container.

Careful examination of Figures 9 and 10 indicates that interfacial evaporation rates depend upon thermal gradients and the extent of dry-out. High thermal gradients result in higher evaporation rates, but thermal gradients are greatest at early times. High moisture content (higher unsaturated hydraulic conductivity) also promotes evaporation, but, once the initial thermal transient is past, higher moisture contents come later in time. The two trends cause interfacial evaporation rates to pass through a maximum with time. The three points in time examined herein are not sufficient to fully describe this trend, however.

A simple calculation is useful to place the interfacial evaporation rates in perspective. The greatest interfacial evaporation rate calculated is 40,000 kg/m/1,000 years. Because the trend is not fully explored with only three points this number is likely to be well below the actual maximum. Nonetheless, it provides a rough estimate of the amount of salt that can be deposited. If the reflux water is assumed to initially have 4,000 mg/L of soluble salts (obtained as a five-fold evaporation of initial pore waters coming from repository wide drying), then this gives 160 kg/m/1,000 years of soluble salts. If the salt solution is at 27.5 percent by weight (solubility of sodium chloride), then 420 kg of water/m can be stabilized over a 1,000 year period. If porosity is 10 percent, then over 4 cubic meters of rock per meter of container length can be saturated over a 1,000 year period. Thus it is possible, even likely, that at late time periods, hygroscopic salts will have an effect on container wetting, although the amounts are not sufficiently great to lead to leachate generation. Additionally, the use of backfill material can lower relative humidity near the waste container sufficiently to prevent hydration of most salts for periods of 10,000 years or more. Dissolution and precipitation of moderately soluble minerals (e.g., silica, calcite) associated with water refluxing near the container will also likely modify transport properties in the host rock near the container.

4. EXAMINATION OF SIMPLIFYING ASSUMPTIONS

The adequacy of the simplifying assumptions for the model depend on the specific application and are considered here for the YM environment. Major simplifying assumptions are: steady state conduction dominated heat transfer, steady state liquid and vapor fluxes, air is assumed to be stagnant, one-dimensional transport, cylindrically symmetric geometry with boundary conditions specified at an arbitrarily chosen outer radius, neglect of large scale buoyancy induced flow of air, constant vapor phase pressure, and simplified constitutive properties at low saturation.

Appropriateness of the assumption of steady state can be estimated using the characteristic times associated with the processes under consideration (Bird et al., 1960). For the quasi-steady state assumption to be valid, the characteristic time to reach a steady state must be short relative to the time scale for changes in boundary conditions and the temperature field. For liquid water flow and water vapor transport, the time to steady state is set by the most rapid response of either transport process. In general at high water saturation, liquid water flow will be more rapid, whereas for more dessicated systems, water vapor transport is more rapid. For the YM simulations, the response time is controlled by vapor transport. Manteufel and Green (1993) analyzed experimental results of two-phase, partially saturated flow in a thermal gradient using a steady-state description and reported good agreement.

The assumption of transport in one-dimension cannot rigorously account for factors such as close spacing of drifts and requires that the container is placed at the center of the drift. Imposition of the outer boundary condition at a distance of 5 m from the waste package is assumed arbitrarily for the waste package scale simulations. Increasing this distance leads to hotter temperatures at the waste package. Large scale buoyancy induced flow of air on the reflux of liquid and vapor is neglected in simulation. This is expected to be a good approximation sufficiently close to the waste package. In addition repository-scale calculations indicate a downward flow of vapor at the repository horizon caused by vapor diffusion in contrast to buoyant driven flow (Tsang and Pruess, 1987; Lichtner and Walton, 1994).

Finally, the constitutive properties used in the simulation to estimate the hydraulic conductivity and diffusivity of water in rock and backfill are limited by both theoretical and experimental considerations. The constitutive relations become more uncertain with increased dry-out of the host rock or backfill. A major conclusion of this work is that, at low saturations, the precise constitutive properties are no longer important. This is a very important conclusion considering the uncertainties in the flux relationships at highly negative matric potentials.

5. SUMMARY

The quasi-steady state model of liquid and vapor transport appears to be a useful tool for exploring the effect of possible combinations of repository-wide thermal loading, individual container thermal loading, and backfill properties on waste package thermohydrology. Other applications are also possible, such as simulation of thermohydrologic conditions below solar ponds and near coils for ground heat pumps. In order to examine model predictions six design scenarios were investigated at three time periods.

The steady-state solution simplifies to constant vapor pressure of water when the dimensionless quantity $\alpha \gg 1$. This limiting case is almost always reached for granular backfill materials. For this reason, backfill materials are anticipated to promote dry conditions near the waste, at least in the absence of buildup of soluble salts. Additionally, for the limiting case, the solution near the waste package depends upon easy-to-measure thermal properties of the backfill materials, but is independent of the precise hydraulic properties of the backfill.

The presence of granular backfill material concentrates maximum evaporation rates at the host rock/backfill interface. In the absence of granular backfill, evaporation is concentrated at the host rock/container surface interface. In fact, because the solution at large r does not depend upon properties at small r, the A and C designs give the same flux and evaporation rates as a design without backfill with a 1.5 m radius cavity. The granular backfill material reduces the liquid matrix flow near the waste to near zero, thereby minimizing soluble salt deposition near the container. However, buildup of hygroscopic salts at the host rock/backfill interface, followed by lower temperatures, could lead to eventual liquid water movement toward the wastes by gravity flow when the salts rehydrate. This situation could be a particular problem if no backfill is present to provide an additional barrier between the rock interface and the container surface. If significant amounts of liquid water ever reach the container, then hygroscopic salts quickly become a major factor in determining continued wetting, water chemistry, and container corrosion (Walton et al., 1994) unless relative humidity is kept very low. For this reason, moving the evaporation front away from the container and lowering the relative humidity by the use of backfill are important to favorable performance of the waste isolation system.

Further work is needed to investigate the sensitivity of the quasi-steady state approach to the outer boundary conditions and the choice of outer radius r_3. In addition the quasi-steady state approach is not expected to apply to modeling a HLW package environment at early times for which a transient description is required because of the rapid change in decay heat.

DISCLAIMER

This work was funded by the U.S. Nuclear Regulatory Commission (NRC). This paper is an independent product under a contract to the Center for Nuclear Waste Regulatory Analyses (CNWRA) and does not necessarily reflect the views or regulatory position of the NRC.

6. REFERENCES

Ali, M. S., King, F. G., and Ilias, S., Diffusive transport of carbon dioxide through USW-G4 Topopah Spring Tuffs, *Mat. Res. Soc.*, *333*, 827-834, 1994.

Bird, R. B., Stewart, W. E., and Lightfoot, E. N., *Transport Phenomena*, John Wiley and Sons, New York, N.Y., 1960.

Buscheck, T. A. and Nitao, J. J., The impact of thermal loading on repository performance at Yucca Mountain, American Nuclear Society, Third High-Level Radioactive Waste Management Conference, Las Vegas, NV, 1003-1017, 1992.

de Vries, D. A., Simultaneous transfer of heat and moisture in porous media, *Transactions, American Geophysical Union*, *39*, No. 5, 909-916, 1958.

Department of Energy, U.S., Multi-purpose canister system evaluation, Washington, DC: U.S. Department of Energy, Office of Civilian Management, DOE/RW-0445, 1994.

Department of Energy, U.S., Yucca Mountain Site Characterization Project Reference Information Base, Revision 2. YMP/93-02. Washington, DC: U.S. Department of Energy, Office of Civilian Radioactive Waste Management, 1993.

Incropera, F. P. and DeWitt, D. P., *Fundamentals of heat and mass transfer*, John Wiley and Sons, New York, N.Y., 919pp, 1990.

Jury, W. A. and Letey, J., Water vapor movement in soil: Reconciliation of theory and experiment, *Soil Science Society of America*, *43*, 1979.

Lichtner, P. C. and Walton, J. C., Near-field liquid-vapor transport in a partially saturated high-level nuclear waste repository, CNWRA 94-022, 1994.

Manteufel, R. D. and Green, R. T., Observations of thermally-driven liquid redistribution in a partially saturated porous medium, *Am. Soc. Mech. Eng.*, *173*, 93–107, 1993.

Nitao, J. J., Numerical modeling of the thermal and hydrological environment around a nuclear waste package using the equivalent conintuum approximation: Horizontal emplacement, *UCID-21444*, Lawrence Livermore National Laboratory, 1988.

Peters, R. R., Klavetter, E. A., Hall, I. J., Blair, S. C., Heller, P. R., and Gee, G. W., Fracture and matrix hydrologic characteristics of tuffaceous materials from Yucca Mountain, Nye County, Nevada, Sandia National Laboratories, Report SAND84-1471, Albuquerque, NM, December (1984).

Press, W. H., Flannery, B. P., Teukolsky, S. A., and Vetterling, W. T., *Numerical Recipes*, Cambridge University Press, 818p, 1986.

Philip, J. R., Adsorption and capillary condensation on rough surfaces, *J. Phys, Chem., 82*, 1379–1385, 1978.

Philip, J. R. and deVries, D. A., Moisture movement in porous materials under temperature gradients, *Transactions, American Geophysical Union, 38*, No. 2, 222-232, 1957.

Pruess, K., Wang, J. S. Y, and Tsang, Y. W., On thermohydrologic conditions near high-level nuclear wastes emplaced in partially saturated fractured tuff 1. Simulation studies with explicit consideration of fracture effects, *Water Resources Research, 26*, 1235-1248, 1990.

Pruess, K. and Tsang, Y., Thermal modeling for a potential high-level nuclear waste repository at Yucca Mountain, Nevada, LBL-35381, UC-600, Lawrence Berkeley Laboratory, Berkeley, CA, 1994.

Tsang, T. W. and Pruess, K. A study of thermally induced convection near a high-level nuclear waste repository in partially saturated fractured tuff, *Water Resources Research, 23*, 1958–1966, 1987.

Udell, K. S., Heat transfer in porous media heated from above with evaporation, condensation, and capillary effects, *Journal of Heat Transfer, 105*, 485–492, 1983.

van Genuchten, M. Th., and Nielsen, D. R., On describing and predicting the hydraulic properties of unsaturated soils, *Annales Geophysicae, 3*, No. 5, 615-628, 1985.

van Genuchten, M., A closed form equation for predicting the hydraulic conductivity of unsaturated soils, *Soil Science Society of America Journal, 44*, 892-898, 1980.

Walton, J. C., Effects of evaporation and solute concentration on presence and composition of water in and around the waste package at Yucca Mountain, *Waste Management, 13*, 293-301, 1993.

Walton, J. C., Influence of evaporation on waste package environment and radionuclide release from a tuff repository, *Water Resources Research, 30*, No. 12, 3479-3487, 1994.

Walton, J. C., Sridhar, N., Cragnolino, G., and Torng, T., An approach to analysis of high level waste container performance in an unsaturated repository environment, *Mat. Res. Soc. Symp. Proc., 333*, 863-867, 1994

Wolfram, S., *Mathematica a system for doing mathematics by computer*, Second edition, Addison-Wesley, New York, 1991.

FIGURE CAPTIONS

Figure 1: Contour plot of the vapor pressure of pure water as a function of temperature and ψ with contour intervals of 0.1 atm.

Figure 2: Contour plot of the ratio of Darcy flux (bulk flow) to diffusive flux for water vapor as a function of temperature and ψ.

Figure 3: Geometry of simulation.

Figure 4: Relative permeability of backfill material and tuff as a function of matric potential (ψ, -m).

Figure 5: Examination of the limiting case simplification for (a) tuff rock and (b) backfill material as a function of temperature and .

Figure 6: Predicted temperature profiles.

Figure 7: Predicted relative humidity.

Figure 8: Predicted mole fraction water vapor.

Figure 9: Predicted water flux (kg/m/s on the left) and evaporation rate (kg/m^2/s on the right) at 28 kW/acre thermal loading.

Figure 10: Predicted water flux (kg/m/s on the left) and evaporation rate (kg/m^2/s on the right) at 57kW/acre thermal loading.

TABLE CAPTIONS

Table 1: Parameters

Table 2: Simulation Geometry

Table 3: Boundary Conditions

Table 4: Simulation Labels

Table 5: Evaporation at Host Rock/Backfill, or Host Rock/Container Boundary

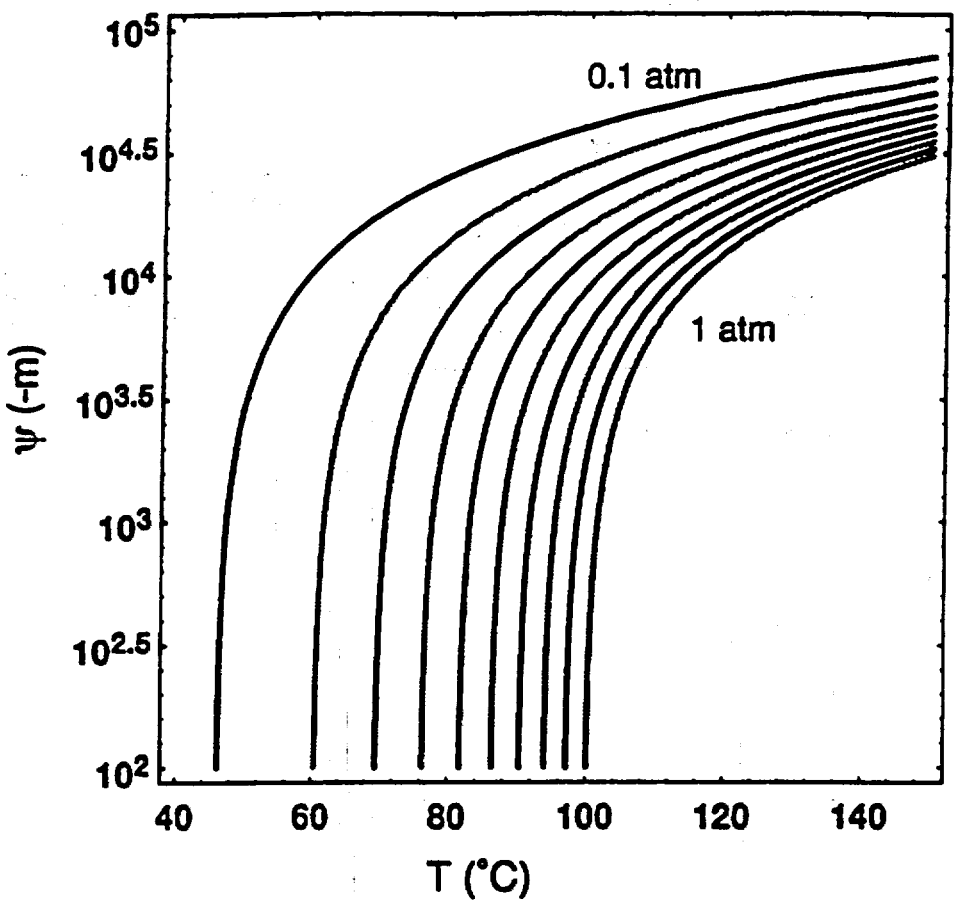
10^5
$10^{4.5}$
10^4
$10^{3.5}$
10^3
$10^{2.5}$
10^2
ψ (-m)
0.1 atm
1 atm
40
60
80
100
120
140
T (°C)

Figure 1

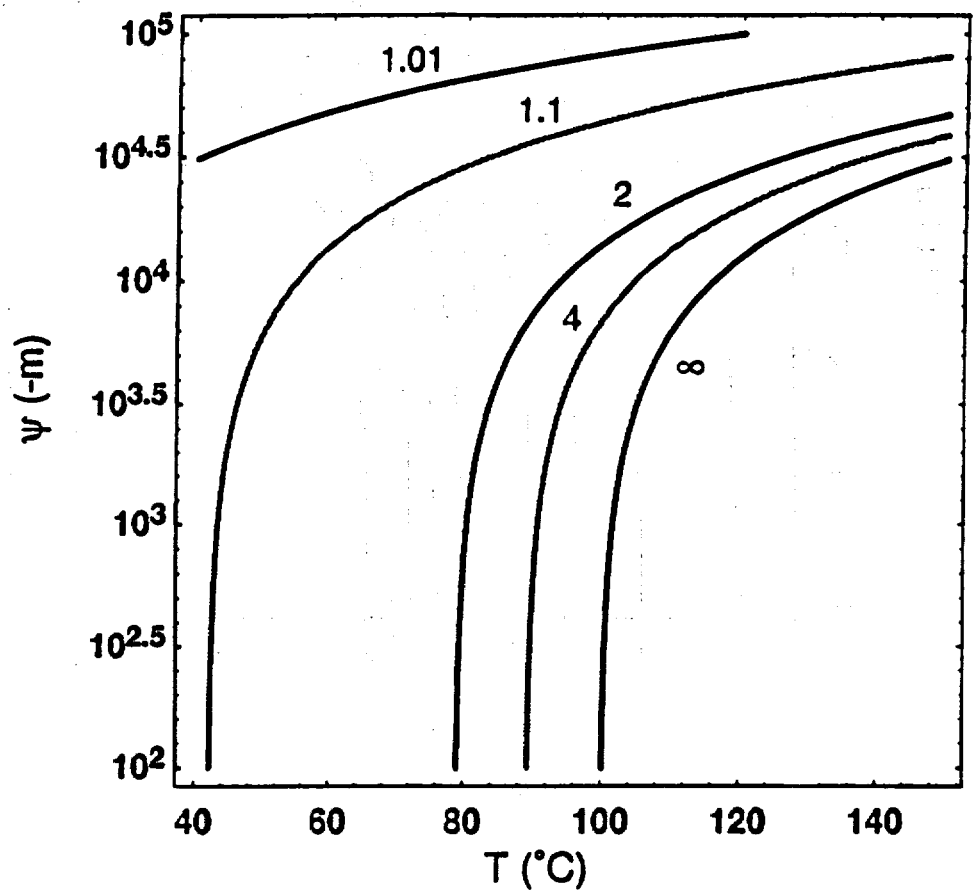
10^5
$10^{4.5}$
10^4
$10^{3.5}$
10^3
$10^{2.5}$
10^2
ψ (-m)
1.01
1.1
2
4
∞
40
60
80
100
120
140
T (°C)

Figure 2

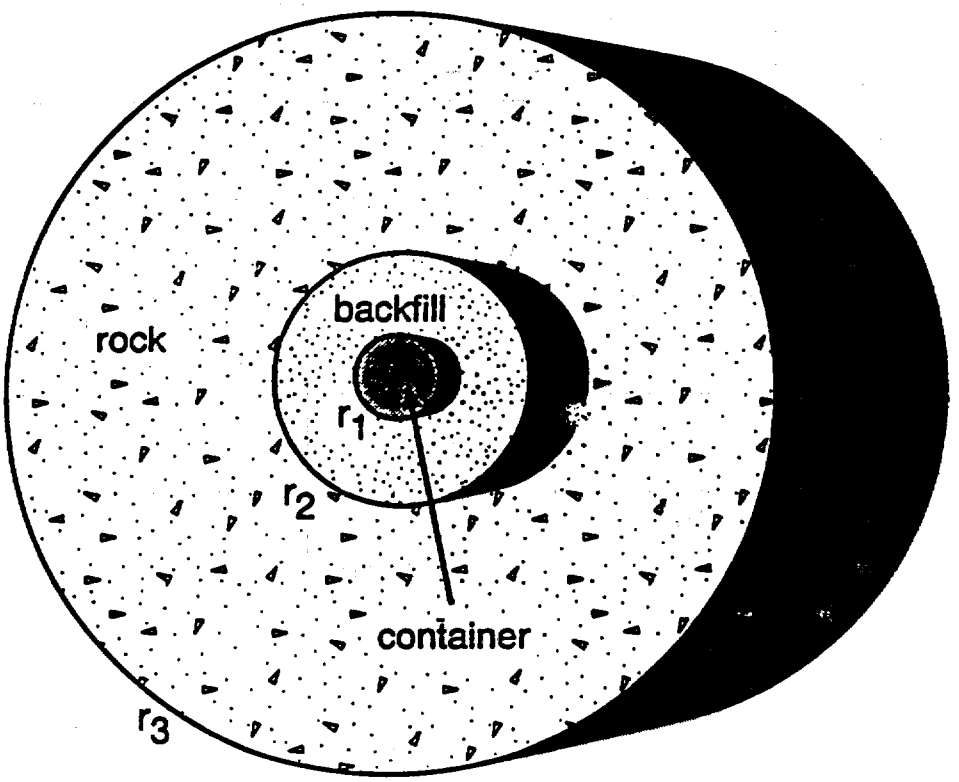

Figure 3

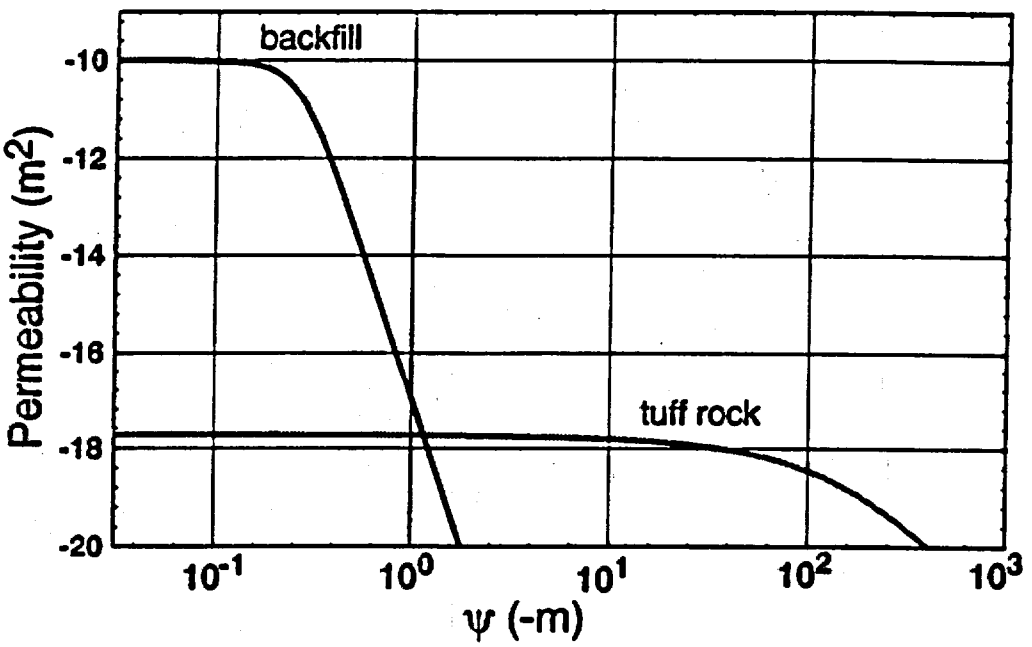
backfill
tuff rock
Permeability (m²)
-10
-12
-14
-16
-18
-20
10⁻¹
10⁰
10¹
10²
10³
ψ (-m)

Figure 4

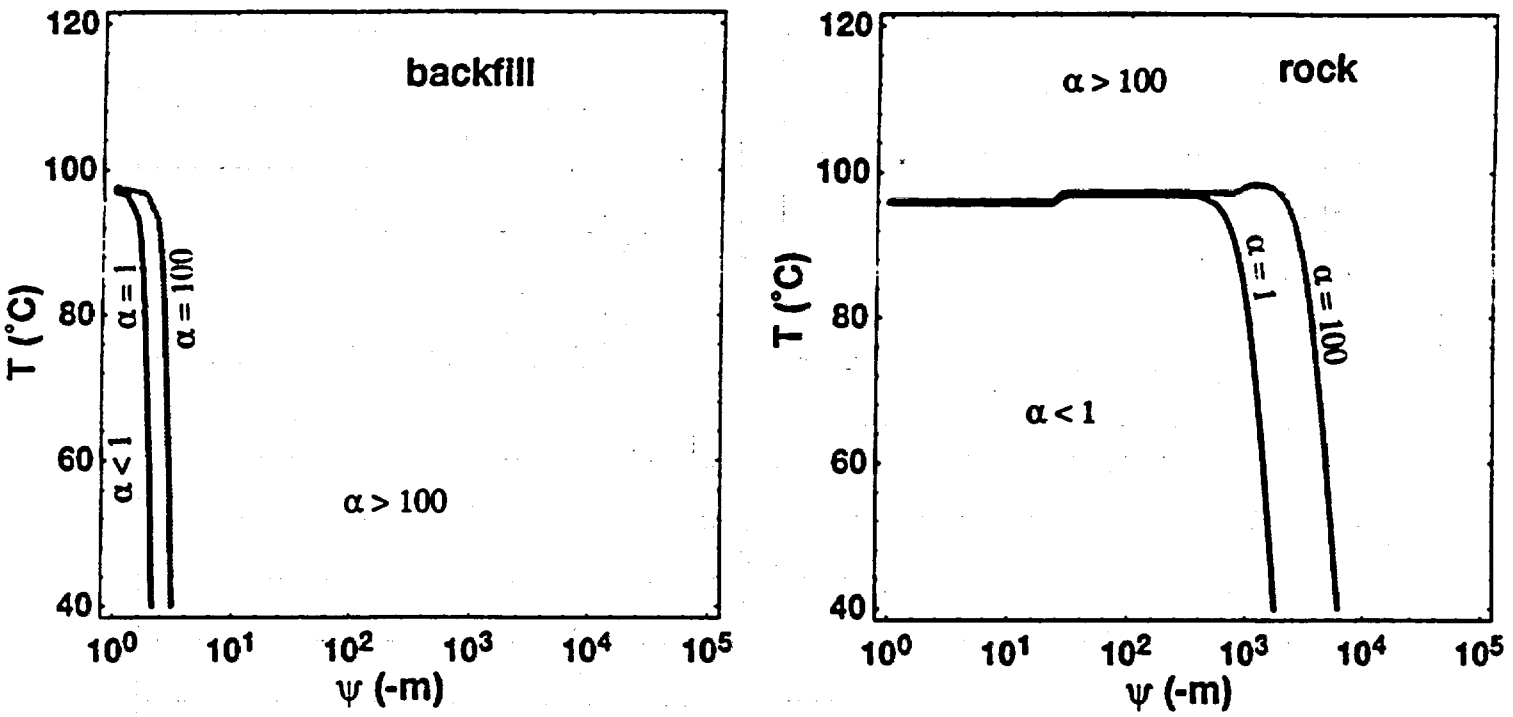
backfill
120
100
80
60
40
T (°C)
α = 1
α = 100
α < 1
α > 100
10^0
10^1
10^2
10^3
10^4
10^5
ψ (-m)
rock
α > 100
α = 1
α = 100
α < 1

Figure 5

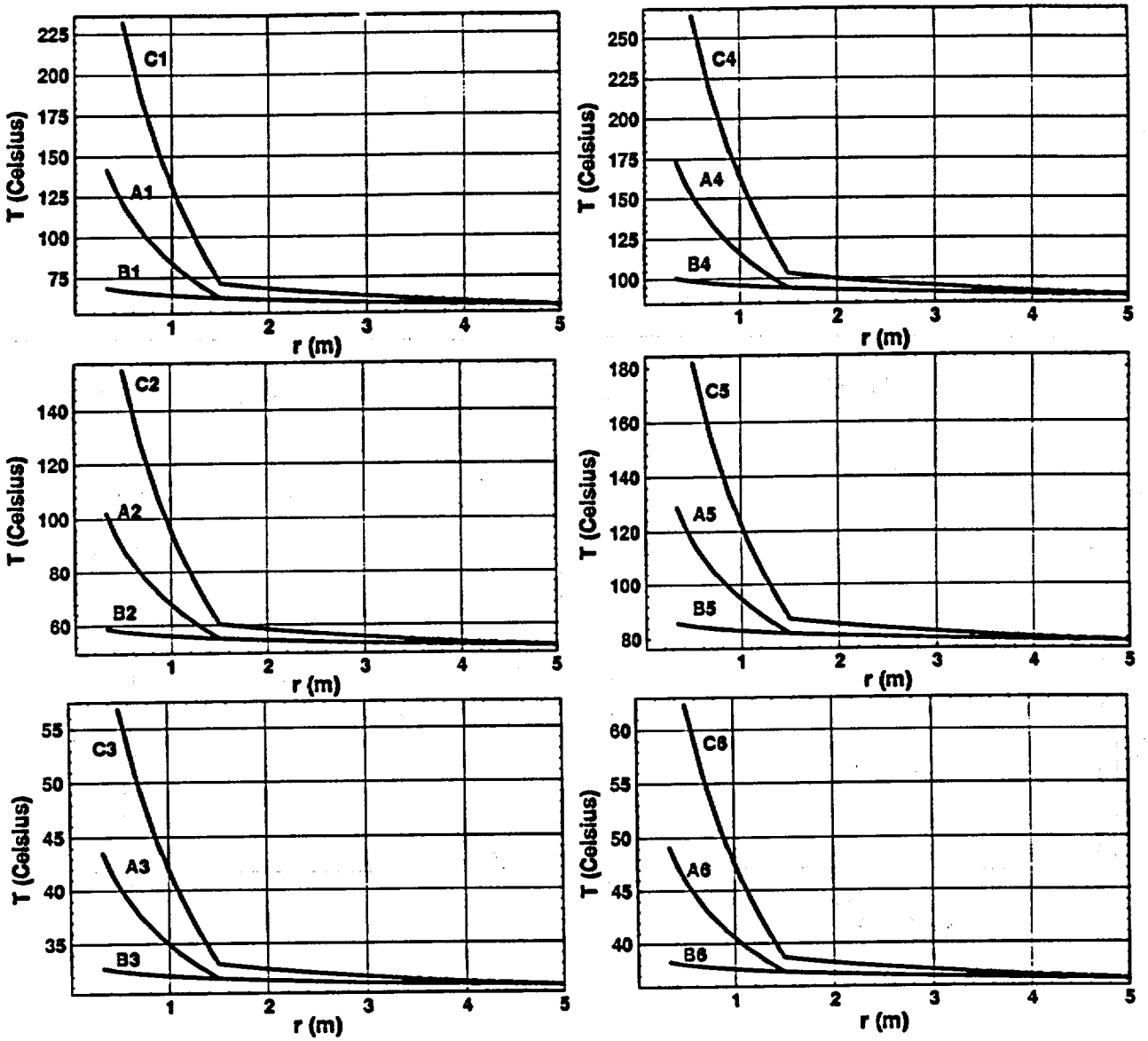

Figure 6

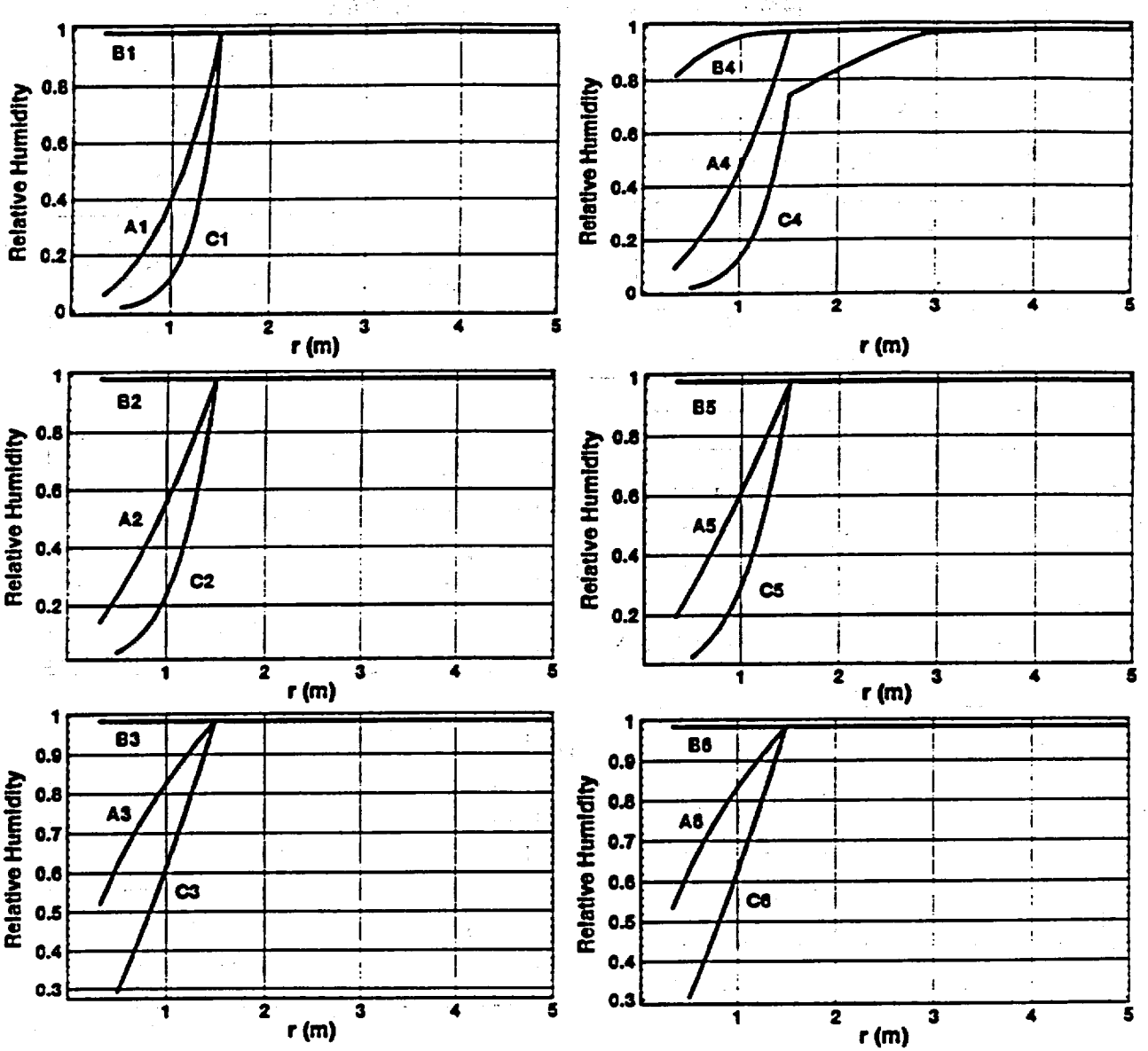
B1
A1
C1
B4
A4
C4
B2
A2
C2
B5
A5
C5
B3
A3
C3
B6
A6
C6
Relative Humidity
r (m)

Figure 7

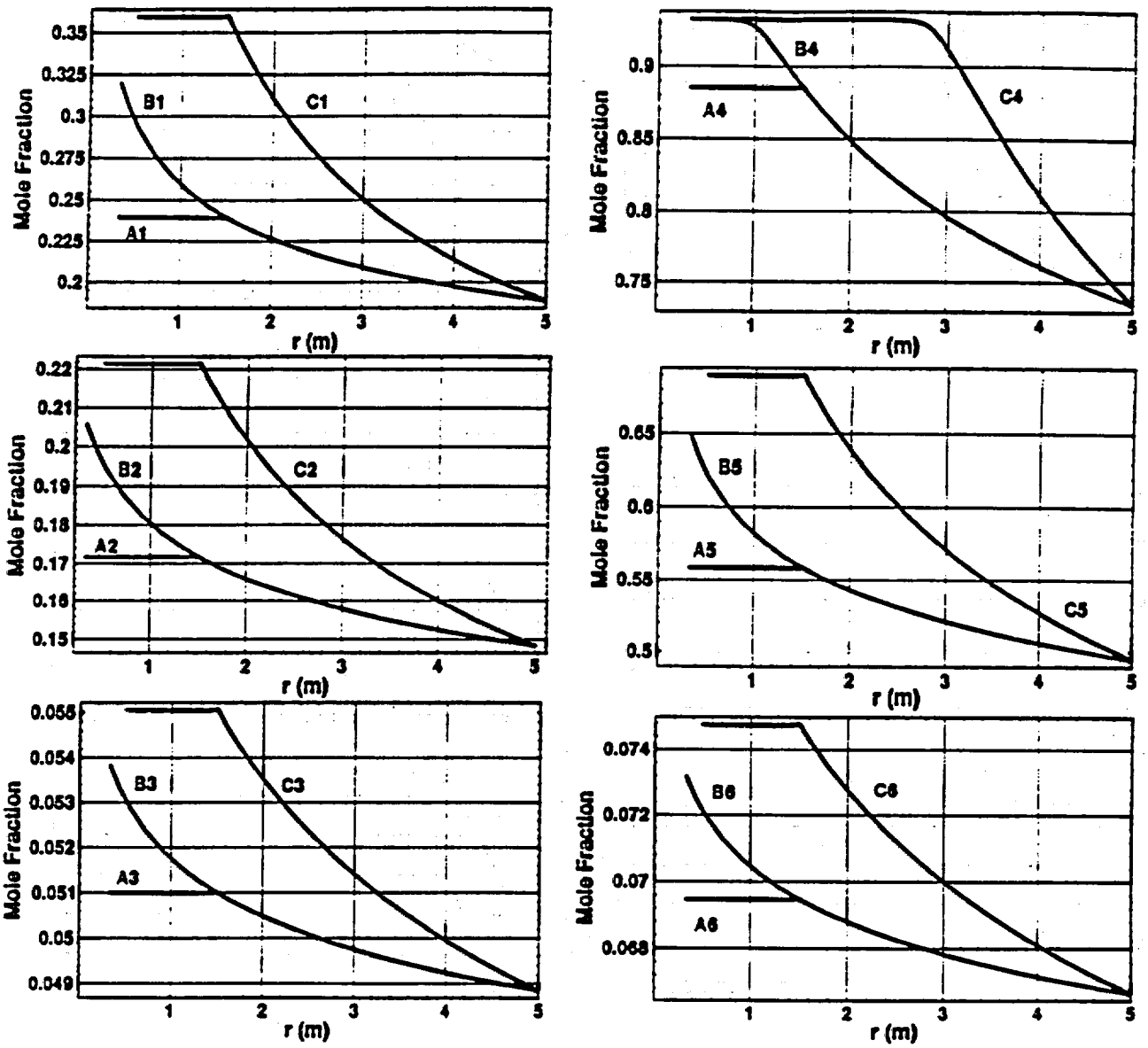
Mole Fraction
r (m)
B1
C1
A1
B4
C4
A4
B2
C2
A2
B5
C5
A5
B3
C3
A3
B6
C6
A6

Figure 8

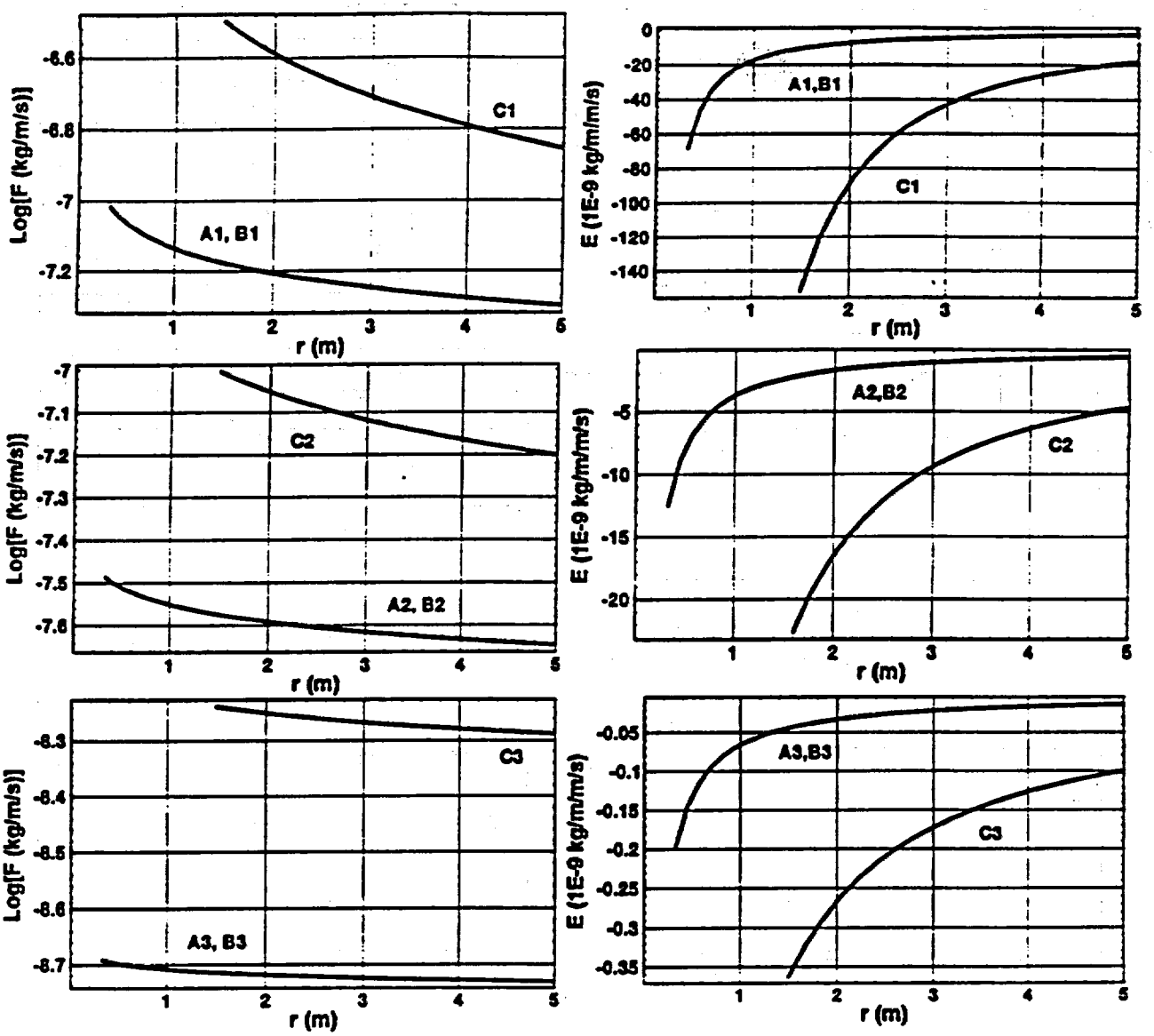
Log[F (kg/m/s)]
-6.6
-6.8
-7
-7.2
C1
A1, B1
1
2
3
4
5
r (m)
E (1E-9 kg/m/m/s)
0
-20
-40
-60
-80
-100
-120
-140
A1,B1
C1
r (m)
Log[F (kg/m/s)]
-7
-7.1
-7.2
-7.3
-7.4
-7.5
-7.6
C2
A2, B2
r (m)
E (1E-9 kg/m/m/s)
-5
-10
-15
-20
A2,B2
C2
r (m)
Log[F (kg/m/s)]
-8.3
-8.4
-8.5
-8.6
-8.7
C3
A3, B3
r (m)
E (1E-9 kg/m/m/s)
-0.05
-0.1
-0.15
-0.2
-0.25
-0.3
-0.35
A3,B3
C3
r (m)

Figure 9

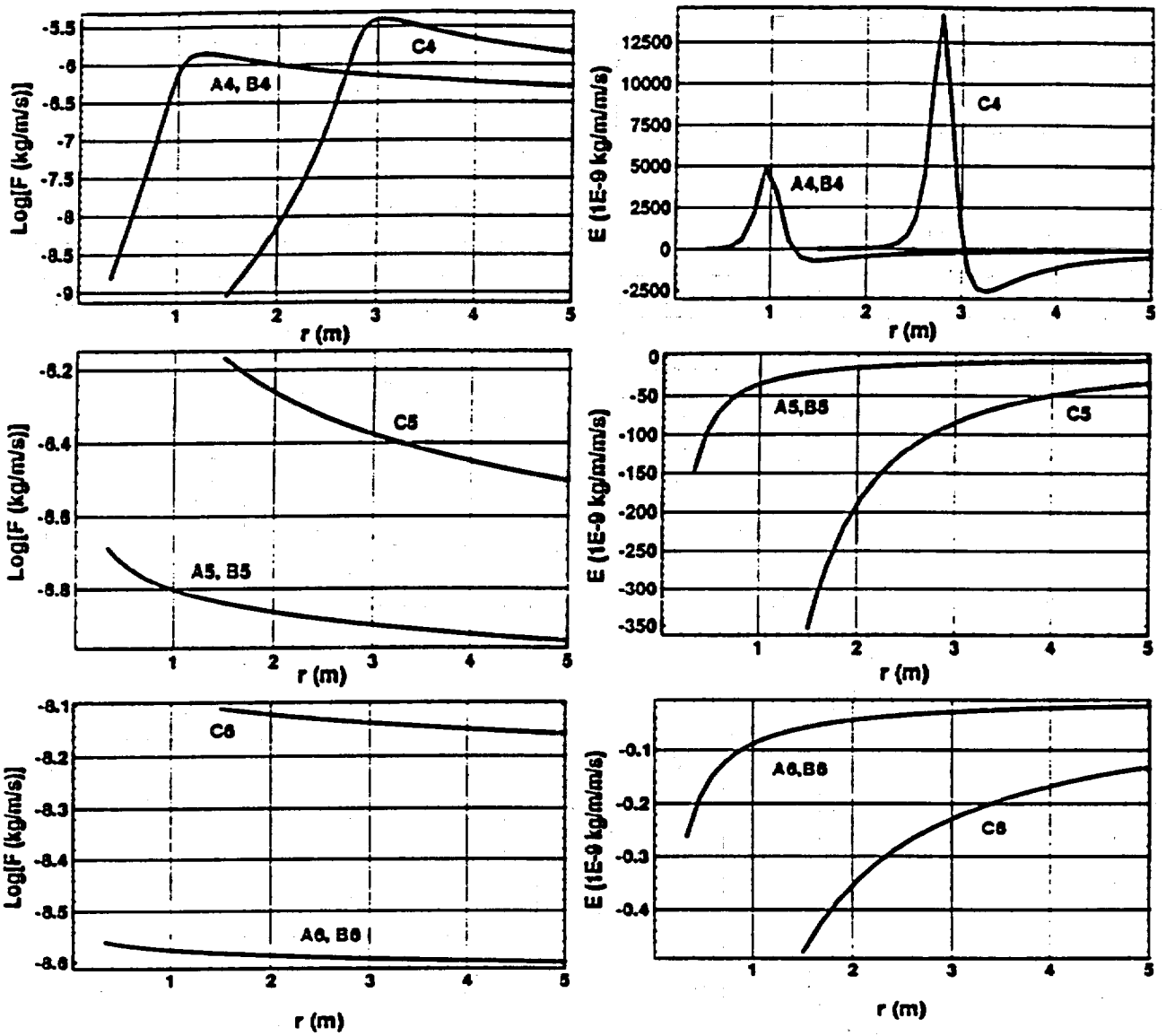

Figure 10

Table 1. Parameters

Parameter	Rock	Backfill
Permeability [m^2]	1.9×10^{-18}	1×10^{-10}
a [m^{-1}]	5.7×10^{-3}	3.64 m^{-1}
n	1.8	5.05
Porosity	0.11	0.37
Thermal Conductivity [J/m/s/K]	1.9	0.155

Table 2. Simulation Geometry

Parameter	A	B	C
Container Radius (m)	0.33	0.33	0.5
Backfill Radius (m)	1.5		1.5
External Boundary (m)	5	5	5

Table 4. Simulation Labels

Thermal Loading (kW/acre)	28.5			57		
Time (yr)	500	1,000	10,000	500	1,000	10,000
Small Container (SCP), Backfill (A)	A1	A2	A3	A4	A5	A6
Small Container (SCP), No Backfill(B)	B1	B2	B3	B4	B5	B6
Multipurpose Canister (MPC), Backfill (C)	C1	C2	C3	C4	C5	C6

Table 3. Time-dependent boundary conditions at the outer radius

Time (yr)	Thermal Loading (kW/acre)	T (°C)	ψ (m)	Q (J/s/m) SCP	Q (J/s/m) MPC
500	57	89	-222	51.1	142
1,000	57	79	-215	30.1	83.7
10,000	57	37	-211	7.55	21.0
500	28.5	57	-195	51.1	142
1,000	28.5	52	-197	30.1	83.7
10,000	28.5	31	-207	7.55	21.0

Table 5. Evaporation at Rock/Backfill Boundary or Rock/Container Boundary

Thermal Loading	28.5 kW/acre			57 kW/acre		
Time (yr)	500	1,000	10,000	500	1,000	10,000
SCP, Backfill	6.6×10^{-8} kg/m/s (2,100 kg/m/1000 yr)	2.5×10^{-8} kg/m/s (840 kg/m/1000 yr)	1.9×10^{-9} kg/m/s (61 kg/m/1000 yr)	1.3×10^{-6} kg/m/s (40,000 kg/m/1000 yr)	1.4×10^{-7} kg/m/s (4,500 kg/m/1000 yr)	2.6×10^{-9} kg/m/s (82 kg/m/1000 yr)
SCP, No Backfill	9.6×10^{-8} kg/m/s (3,000 kg/m/1000 yr)	3.3×10^{-8} kg/m/s (1,000 kg/m/1000 yr)	2.0×10^{-9} kg/m/s (64 kg/m/1000 yr)	1.7×10^{-9} kg/m/s (54 kg/m/1000 yr)	2.0×10^{-7} kg/m/s (6,400 kg/m/1000 yr)	2.8×10^{-9} kg/m/s (87 kg/m/1000 yr)
MPC, Backfill	3.2×10^{-7} kg/m/s (10,000 kg/m/1000 yr)	9.9×10^{-8} kg/m/s (3,100 kg/m/1000 yr)	5.8×10^{-9} kg/m/s (180 kg/m/1000 yr)	9.4×10^{-10} kg/m/s (30 kg/m/1000 yr)	6.8×10^{-7} kg/m/s (21,300 kg/m/1000 yr)	7.8×10^{-9} kg/m/s (250 kg/m/1000 yr)